Two-dimensional Legendre polynomial modeling of composite bulk acoustic wave resonators

Cite as: J. Appl. Phys. **108**, 104904 (2010); https://doi.org/10.1063/1.3504611
Submitted: 16 June 2010 • Accepted: 21 September 2010 • Published Online: 18 November 2010

A. Raherison, J. E. Lefebvre, F. E. Ratolojanahary, et al.

Two-dimensional Legendre polynomial modeling of composite bulk acoustic wave resonators

A. Raherison,[1] J. E. Lefebvre,[2,a)] F. E. Ratolojanahary,[1] L. Elmaimouni,[3] and T. Gryba[2]
[1]*LAPAUF, Université de Fianarantsoa, 301 Fianarantsoa, Madagascar*
[2]*Univ Lille Nord de France, F-59000 Lille, France; UVHC, IEMN-DOAE, 59313 Valenciennes Cedex 9, France; and CNRS, UMR 8520, F-59650 Villeneuve d'Ascq, France*
[3]*ERSITA, Faculté polydisciplinaire d'Ouarzazate, Université Ibn Zohr, 45000 Ouarzazate, Morocco*

(Received 16 June 2010; accepted 21 September 2010; published online 18 November 2010)

A bidimensional analysis of 6 mm hexagonal resonators is described using a double orthonormal basis set for the expansion of field quantities. The analysis takes into account the electrical voltage source and by means of a unique formalism along with a single calculation restitutes all the types of resonance whatever the thickness to width ratio value through either modal solutions or electrical impedance. An illustrative example gives the capabilities of the method to investigate spurious modes in laterally bounded resonators. © *2010 American Institute of Physics*.
[doi:10.1063/1.3504611]

I. INTRODUCTION

The demand for monolithic integration of acoustic wave resonators as core components in mobile communication systems call for efficient tools of simulation. One-dimensional (1D) models allow only a partial description of resonator's performances. A full description requires to take into account the finite lateral dimensions of the resonator what can be done with two-dimensional (2D) and/or three-dimensional analytical models.[1–4] However, these models are computationally intensive, time consuming, and require a large amount of memory space. Thus, semianalytical models are highly desirable. We propose here a Legendre polynomial-based 2D semianalytical approach able to take into account a finite lateral dimension.

Up to now, the Legendre polynomial method was only applied to 1D modeling.[5] An extended formulation is presented here for 2D modeling. The method uses constitutive and propagation equations to describe the structure. The boundary conditions and the electrical source are incorporated into the field equations and are automatically accounted for.[5,6] The equations are solved by expanding each mechanical displacement component and electrical potential in a double series made up of products of Legendre polynomials. Both the harmonic and modal analyses are then studied through a unique formalism.[5,6]

In Sec. II, the mathematical modeling is described in detail. The resolution method that allows reducing the computing time and improving the calculation accuracy is given. In Sec. III, the method is applied for validation to well-known cases where solutions are available either in literature or through approached analytical models or in literature for Lead Zirconate Titanate PZT5H. Then a ZnO homogeneous resonator is considered as illustrative example in order to emphasize the capabilities of the method. A brief conclusion is given in Sec. IV.

II. MATHEMATICAL FORMULATION

A. Structure

The studied structure is a piezolayer sandwiched between two infinitely thin electrodes assumed to be perfect conductors, driven by a voltage source as shown in Fig. 1. The coordinate axes x_1, x_2, and x_3 coincide with the crystal axes X, Y, and Z and the x_3 axis is normal to the layer. The media occupies the space $-L_1/2 \leq x_1 \leq +L_1/2$, $-L_3/2 \leq x_3 \leq +L_3/2$ and is assumed to be infinite along x_2–direction. It is characterized by its mass density, ρ, stiffness tensor at constant electric field, c, elastic viscosity tensor, η, piezoelectric tensor, e, and permittivity tensor at constant strain, ε. Superscripts E on c and S on ε are omitted for simplicity. Throughout this paper, $\exp(i\omega t)$ time dependence is implicit.

B. Constitutive equations

Within the piezoelectric material, an electromechanical coupling phenomenon occurs. This phenomenon is defined by the constitutive equations:

$$T_{ac} = c_{acbd}\frac{\partial u_b}{\partial x_d} + e_{dac}\frac{\partial \phi}{\partial x_d}, \tag{1a}$$

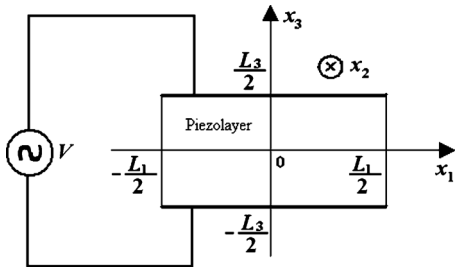

FIG. 1. Schematic view of the resonator.

a)Electronic mail: jean-etienne.lefebvre@univ-valenciennes.fr.

$$D_c = e_{cbd}\frac{\partial u_b}{\partial x_d} - \varepsilon_{cd}\frac{\partial \phi}{\partial x_d}, \tag{1b}$$

where u_b represents the components of particle displacement, T_{ac} and D_c are the stress and electrical displacement, and ϕ is the electric potential. The subscripts a, b, c, and d take on the values 1, 2, and 3 and summation over repeated subscripts is implied throughout this paper, unless otherwise specified.

C. Equations of motion

The field equations governing wave propagation in piezoelectric media are given by:

$$\frac{\partial T_{ac}^S}{\partial x_c} = -\rho^S \omega^2 u_a, \tag{2a}$$

$$\frac{\partial D_c^S}{\partial x_c} = 0, \tag{2b}$$

where the superscript s denotes the global structure.

The boundary conditions require that: (i) the normal component of the stress should be zero at the mechanically free surfaces; (ii) the normal component of the electrical displacement should be zero at the lateral surfaces; (iii) the component of the electrical displacement should be free at the metalized surfaces. The changes in variables $q_1 = (2x_1/L_1)$ and $q_3 = (2x_3/L_3)$ are introduced for mathematical convenience.

D. Analytical solutions

In order (i) to describe the structure and (ii) to automatically incorporate the boundary conditions at the outer surfaces,[5,6] the rectangular window function Π defined as follows:

$$\Pi(q_c) = \begin{cases} 1 & if \quad -1 < q_c < 1 \\ 0 & \text{otherwise} \end{cases}, \tag{3}$$

is introduced into the propagation Eqs. (2a) and (2b).This gives:

$$\frac{2}{L_c}\frac{\partial}{\partial q_c}[T_{ac}\Pi(q_1)\Pi(q_3)] = -\omega^2 \rho \Pi(q_1)\Pi(q_3)u_a, \tag{4a}$$

$$\frac{2}{L_c}\frac{\partial}{\partial q_c}\{D_c\Pi(q_1)[\delta_{c1} + \delta_{c3}\Pi(q_3)]\} = 0, \tag{4b}$$

where δ_{ab} is the Kronecker symbol defined as:

$$\delta_{ab} = \begin{cases} 1 & if \quad a = b, \\ 0 & if \quad a \neq b. \end{cases} \tag{5}$$

The derivatives of the rectangular window functions give rise to delta functions $\delta(q_a \pm 1)$ multiplying the normal electric displacement component at lateral surfaces and the normal stress component at the mechanically free surfaces thus ensuring that $D_1(q_1 = \pm 1) = 0$ and $T_{ac}(q_a = \pm 1) = 0$.

For mathematical and programming convenience, we adopt the normalized physical constants:

$$\bar{c}_{acbd} = \frac{c_{acbd}}{c_{33}^D}, \quad \bar{\eta}_{acbd} = \frac{\eta_{acbd}\omega_L}{c_{33}^D},$$

$$\bar{e}_{cbd} = \frac{e_{cbd}}{\sqrt{c_{33}^D \varepsilon_{33}}}, \quad \bar{\varepsilon}_{cd} = \frac{\varepsilon_{cd}}{\varepsilon_{33}},$$

where ω_L is the 1D thickness resonance angular frequency:

$$\omega_L = \frac{\pi}{L_3}\sqrt{\frac{c_{33}^D}{\rho}} \quad \text{and} \quad c_{33}^D = c_{3333} + \frac{e_{333}^2}{\varepsilon_{33}}.$$

We also assume that the crystal of the piezolayer is a hexagonal 6 mm class crystal with a complex normalized elastic stiffness $\bar{c}'_{acbd} = \bar{c}_{acbd} + i\bar{\eta}_{acbd}\Omega$ where Ω denotes the normalized angular frequency defined by $\Omega = \omega/\omega_L$.

Under these conditions, substituting Eqs. (1a) and (1b) into Eqs. (4a) and (4b) gives:

$$\frac{L_3}{L_c}\frac{\partial}{\partial q_c}\left\{\left[\frac{L_3}{L_d}\bar{c}'_{acbd}\frac{\partial \bar{u}_b}{\partial q_d} + \frac{1}{r}\frac{L_3}{L_d}\bar{e}_{dac}\frac{\partial \phi}{\partial q_d}\right]\Pi(q_1)\Pi(q_3)\right\} = -\frac{\Pi^2}{4}\Omega^2 \bar{u}_a \Pi(q_1)\Pi(q_3) \tag{6a}$$

$$\frac{L_3}{L_c}\frac{\partial}{\partial q_c}\left\{\left[r\frac{L_3}{L_d}\bar{e}_{cbd}\frac{\partial \bar{u}_b}{\partial q_d} - \frac{L_3}{L_d}\bar{\varepsilon}_{cd}\frac{\partial \phi}{\partial q_d}\right] \times \Pi(q_1)[\delta_{c1} + \delta_{c3}\Pi(q_3)]\right\} = 0 \tag{6b}$$

with $r = 10^{-10}\sqrt{c_{33}^D/\varepsilon_{33}}$ [V Å^{-1}] and $\bar{u}_a = u_a[m] \times 10^{10}$. Moreover, the subscripts a, b, c, and d take on only the values 1 and 3.

Since the field quantities are assumed to exist only within the structure, they may be expanded in terms of a complete orthonormal set of functions chosen according to the geometry of the structure. Therefore, the mechanical displacement components and the electric potential are expanded as follows:

$$\bar{u}_b(q_1, q_3) = p_{mn}^b Q_m(q_1) Q_n(q_3), \tag{7a}$$

$$\phi(q_1, q_3) = \frac{V}{2}q_3^3 + (q_3^2 - 1)r_{mn}Q_m(q_1)Q_n(q_3), \tag{7b}$$

with

$$Q_k(q_a) = \sqrt{\frac{2k+1}{2}}P_k(q_a),$$

where P_k denotes the kth Legendre polynomial. The expansion coefficients p_{mn}^b and r_{mn} are in angstrom and in volt, respectively. The electric potential (7b) is expressed in such a way that allows to automatically incorporate the electric source $\phi(q_3 = 1) - \phi(q_3 = -1) = V$ in the propagation equations and where the r_{mn}'s are devoted to fitting of the electric potential gradient within the structure.[5]

Substituting the particle displacement (7a) and electric potential (7b) into Eqs. (6a) and (6b), multiplying by Q_j and Q_k and integrating over q_1 and q_3 from -1 to $+1$, we finally obtain an infinite system of linear equations with p_{mn}^b as unknowns and Ω as parameter:

$$-\Omega^2 MM_{jkmn} p^a_{mn} = (AA^{ab}_{jmkn} + i\Omega NN^{ab}_{jmkn}) p^b_{mn} + BB^a_{jmkn} r_{mn} + EE^a_{jk} V, \tag{8a}$$

$$CC^b_{jmkn} p^b_{mn} - DD_{jmkn} r_{mn} - FF_{jk} V = 0. \tag{8b}$$

The matrices MM_{jkmn}, NN^{ab}_{jmkn}, AA^{ab}_{jmkn}, BB^a_{jmkn}, CC^b_{jmkn}, DD_{jmkn}, EE^a_{jk}, and FF_{jk} are evaluated in Appendix.

Substituting Eqs. (8b) into (8a) yields:

$$(AA^{ab}_{jmkn} + BB^a_{jmkn} DD^{-1}_{jmkn} CC^b_{jmkn} + i\Omega NN^{ab}_{jmkn}) p^b_{mn} + (EE^a_{jk} - BB^a_{jmkn} DD^{-1}_{jmkn} FF_{jk}) V = -\Omega^2 MM_{jmkn} p^a_{mn}. \tag{9}$$

According to Ampere's law, the displacement current density through the piezolayer is:

$$J(q_1, q_3) = i\omega D_3(q_1, q_3), \tag{10a}$$

and the current that flows through the metallic electrode of area S is given by:

$$I(q_3) = -i\omega \int\int_{(S)} D_3(q_1, q_3) dS. \tag{10b}$$

Using the expression of D_3 defined in (1b), and calculating the spatial average current I over the piezolayer thickness, we obtain:

$$I = iC_0\omega \left(V - \frac{r}{2} GG^b_{mn} p^b_{mn} \right), \tag{10c}$$

where $C_0 = \varepsilon_{33}/\zeta$ is the static capacitance with $\zeta = L_1/L_3$, p^b_{mn} is the solution of (9), and the factor GG^b_{mn} is evaluated as indicated in the Appendix.

1. Harmonic analysis

Our goal is to calculate the electric input admittance of the micro electromechanical system (MEMS) resonator Y expressed in a normalized form:

$$\bar{Y} = Y/iC_0\omega, \tag{11}$$

with $Y = I/V$.

Dividing the electric current I in (10c) by the applied voltage V, the normalized electric input admittance is given by:

$$\bar{Y} = 1 - \frac{r}{2V} GG^b_{mn} p^b_{mn}. \tag{12}$$

2. Modal analysis

The aim is to find out the resonance and antiresonance frequencies and the associate field profiles within the structure. Modal analysis is a specific case of harmonic analysis obtained by canceling the electric source voltage. Since the resonance frequencies do not depend on the viscosity tensor,[7] we can simplify the problem by considering a lossless resonator ($\eta = 0$ thus $NN^{ab}_{jmkn} = 0$).

(1) Normalized resonance frequencies:

To obtain the normalized series resonance frequencies Ω_r, we turn off the voltage source ($V = 0$) in (9). This yields:

$$\Omega_r^2 \delta_{ba} p^b_{mn} = -[MM_{jmkn}]^{-1} (AA^{ab}_{jmkn} + BB^a_{jmkn} DD^{-1}_{jmkn} CC^b_{jmkn}) p^b_{mn}. \tag{13}$$

(2) Normalized antiresonance frequencies:

Similarly, to find out the normalized antiresonance frequencies Ω_p, the electric current source should be vanished ($I = 0$). Consequently, (10c) becomes:

$$V = \frac{r}{2} GG^b_{mn} p^b_{mn}. \tag{14}$$

Substituting (14) into (9), the normalized antiresonance frequencies Ω_p are given by:

$$\Omega_p^2 \delta_{ba} p^b_{mn} = -[MM_{jmkn}]^{-1} \left(AA^{ab}_{jmkn} + BB^a_{jmkn} DD^{-1}_{jmkn} CC^b_{jmkn} + \frac{r}{2} HH^a_{jk} GG^b_{mn} \right) p^b_{mn}. \tag{15}$$

with $HH^a_{jk} = EE^a_j - BB^a_{jmkn} DD^{-1}_{jmkn} FF_j$.

In both cases, the eigenvectors p^b_{mn} allow the field profiles associated to the resonance and anti-resonance frequencies to be calculated.

III. NUMERICAL RESULTS

The fields are expanded in an infinite series of orthonormal polynomials. In practice, the infinite summations are truncated to finite values M and N when higher-order terms become essentially negligible. Depending on the analysis type, the problem requires a system of $(M+1)\times(N+1)$ linear equations with $(M+1)\times(N+1)$ unknowns for the harmonic analysis or an eigenvalue system with $(M+1)\times(N+1)$ eigenmodes for the modal analysis to be solved. The solutions to be accepted are those for which convergence is obtained as M and N are increased.[8–11]

In order to reduce the computational time and to improve the calculation accuracy, the symmetry of fields is exploited.[11]

A. Approach validation

In order to check the effectiveness of the proposed model and to validate our computer program, it is applied to solving problems with geometrical configurations where approached analytical solutions are easy to establish or where solutions are available in literature. Modes are calculated for a ZnO resonator with four geometries:

(1) A ZnO homogeneous resonator with $\zeta = 0$ (1D case);
(2) A ZnO homogeneous resonator with $\zeta \ll 1$ (thin plate case);
(3) A ZnO homogeneous resonator with $\zeta \gg 1$ (bar case);
(4) A PZT5H homogeneous resonator with $L_1 = 1.53$ mm and $L_3 = 0.7$ mm.[12]

In every case, the normalized electric input admittance is presented and compared with that of the approached analytical method.[11] For the first three geometries, the resonance and antiresonance frequencies are also given and compared

TABLE I. The material constants used in simulations.

Parameters	Symbols	ZnO
Mass density (10^3 kg m^{-3})	ρ	5.676
Elastic stiffness (10^{10} N m^{-2})	c	$\begin{bmatrix} 20.97 & 12.11 & 10.51 & 0 & 0 & 0 \\ 12.11 & 20.97 & 10.51 & 0 & 0 & 0 \\ 10.51 & 10.51 & 21.09 & 0 & 0 & 0 \\ 0 & 0 & 0 & 4.25 & 0 & 0 \\ 0 & 0 & 0 & 0 & 4.25 & 0 \\ 0 & 0 & 0 & 0 & 0 & 4.43 \end{bmatrix}$
Elastic viscosity (10^{-3} Pa s)	η	$\begin{bmatrix} 11.96 & 11.02 & 11.02 & 0 & 0 & 0 \\ 11.02 & 11.96 & 11.02 & 0 & 0 & 0 \\ 11.02 & 11.02 & 11.96 & 0 & 0 & 0 \\ 0 & 0 & 0 & 0.472 & 0 & 0 \\ 0 & 0 & 0 & 0 & 0.472 & 0 \\ 0 & 0 & 0 & 0 & 0 & 0.472 \end{bmatrix}$
Piezoelectric constant (C m^{-2})	e	$\begin{bmatrix} 0 & 0 & 0 & 0 & -0.59 & 0 \\ 0 & 0 & 0 & -0.59 & 0 & 0 \\ -0.61 & -0.61 & 1.14 & 0 & 0 & 0 \end{bmatrix}$
Permittivity (10^{-10} F m^{-1})	ε	$\begin{bmatrix} 0.738 & 0 & 0 \\ 0 & 0.738 & 0 \\ 0 & 0 & 0.783 \end{bmatrix}$

with the analytically determined ones. The associated relative accuracy is calculated as follows for, respectively, the resonant and antiresonance normalized frequencies:

$$\varepsilon_r(\%) = 100\left|\frac{(\Omega_r)_{an} - (\Omega_r)_{pol}}{(\Omega_r)_{an}}\right|, \tag{16a}$$

$$\varepsilon_p(\%) = 100\left|\frac{(\Omega_p)_{an} - (\Omega_p)_{pol}}{(\Omega_p)_{an}}\right|, \tag{16b}$$

where the subscripts *an* and *pol* represent the analytical and polynomial results, respectively. The material constants used in simulations are shown in Table I.

1. A ZnO homogeneous resonator with $\zeta=0$: 1D case

In the case, $\zeta=0$, we check out the capability of the method to restitute the 1D thickness resonances (see Fig. 2 and Tables II and III).

2. A ZnO homogeneous resonator with $\zeta \ll 1$: Thin plate case

In the case, $\zeta \ll 1$, we check out the capability of the approach to restitute the lateral resonances (see Fig. 3 and Tables IV and V).

As the lateral dimension is much greater than the thickness one, we obtain very low normalized frequencies.

3. A ZnO homogeneous resonator with $\zeta \gg 1$: Bar case

In this case, with $\zeta \gg 1$, as the lateral dimension is much smaller than the thickness one, we obtain normalized frequencies in the same range as thickness resonance frequencies (see Fig. 4 and Tables VI and VII).

The Tables II–VII and the Figs. 2–4 illustrate the normalized resonance and antiresonance frequencies and normalized admittances of resonator. Agreement between ap-

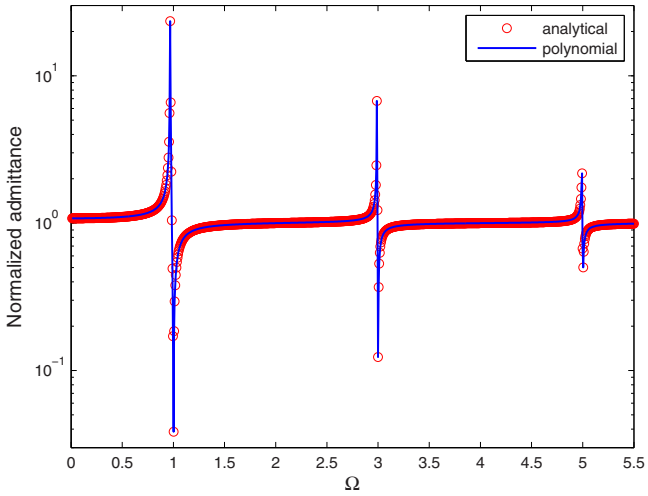

FIG. 2. (Color online) 1D Normalized admittance of ZnO resonator ($\zeta=0$: 1D case).

TABLE II. 1D normalized resonance frequency of ZnO resonator (ζ=0).

Modes	$(\Omega_r)_{an}$	$(\Omega_r)_{pol}$	ε_r (%)
1	0.9695	0.9695	0.00
3	2.9901	2.9901	0.00
5	4.9941	4.9941	0.00
7	6.9958	6.9958	0.00
9	8.9967	8.9967	0.00

TABLE III. 1D normalized antiresonance frequency of ZnO resonator (ζ=0).

Modes	$(\Omega_p)_{an}$	$(\Omega_p)_{pol}$	ε_p (%)
1	1.00	1.00	0.00
3	3.00	3.00	0.00
5	5.00	5.00	0.00
7	7.00	7.00	0.00
9	9.00	9.00	0.00

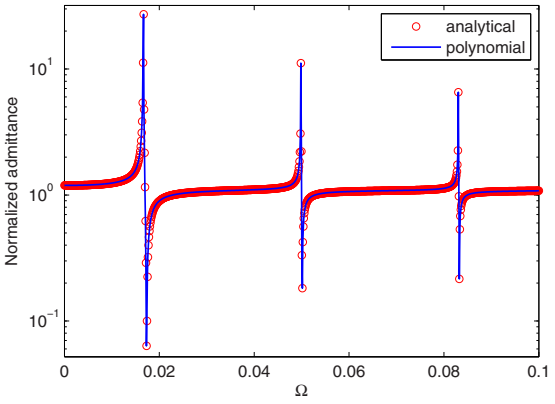

FIG. 3. (Color online) Normalized admittance of ZnO resonator (ζ=0.02: thin plate case).

TABLE IV. Normalized resonance frequency of ZnO resonator (ζ=0.02).

Modes	$(\Omega_r)_{an}$	$(\Omega_r)_{pol}$	ε_r (%)
1	0.0166	0.0166	0.00
3	0.0499	0.0499	0.00
5	0.0832	0.0832	0.00
7	0.1164	0.1164	0.00
9	0.1497	0.1497	0.00

TABLE V. Normalized antiresonance frequency of ZnO resonator (ζ=0.02).

Modes	$(\Omega_p)_{an}$	$(\Omega_p)_{pol}$	ε_p (%)
1	0.0173	0.0173	0.00
3	0.0519	0.0519	0.00
5	0.0865	0.0865	0.00
7	0.1211	0.1211	0.00
9	0.1558	0.1558	0.00

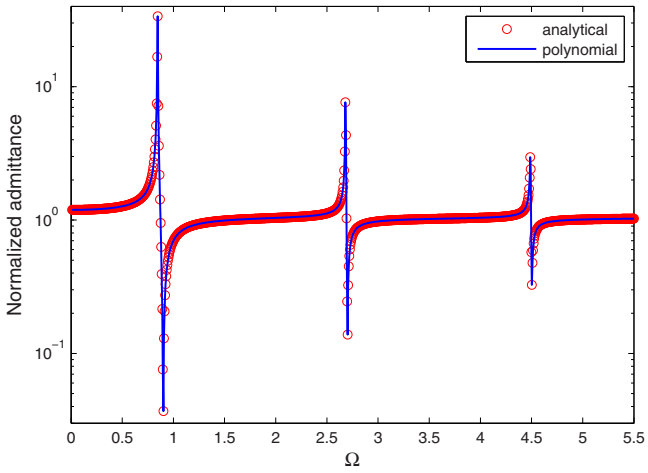

FIG. 4. (Color online) Normalized admittance of ZnO resonator (ζ=200: bar case).

TABLE VI. Normalized resonance frequency of ZnO resonator (ζ=200).

Modes	$(\Omega_r)_{an}$	$(\Omega_r)_{pol}$	ε_r (%)
1	0.8453	0.8453	0.00
3	2.5359	2.5359	0.00
5	4.2264	4.2264	0.00
7	5.9170	5.9170	0.00
9	7.6076	7.6076	0.00

TABLE VII. Normalized antiresonance frequency of ZnO resonator (ζ=200).

Modes	$(\Omega_p)_{an}$	$(\Omega_p)_{pol}$	ε_p (%)
1	0.9001	0.9001	0.00
3	2.7004	2.7004	0.00
5	4.5006	4.5006	0.00
7	6.3010	6.3010	0.00
9	8.1012	8.1012	0.00

TABLE VIII. Resonance and antiresonance frequencies of PZT5H resonator.

Results	Modes	Resonance (MHz)	Antiresonance (MHz)
Experimental[a]	1	0.91	1.22
	3	2.45	2.51
Theoretical[a]	1	0.99	1.29
	3	2.47	2.49
Polynomial	1	0.94	1.26
	3	2.43	2.46

[a]Reference 12.

proached analytical results and our 2D polynomial results is quite good. This validates our model and our software program for extreme geometries.

4. A PZT5H homogeneous resonator with L_3=0.7 mm and L_1=1.53 mm

With this example, we check out the capability of our approach to restitute the resonances for an intermediate geometry.

The Table VIII shows the resonance and antiresonance frequencies of a 0.7 mm thick and 1.53 mm wide PZT5H resonator. Here again, comparison of our polynomial results against the experimental and theoretical ones taken from literature reveals a very good agreement.

The good agreement for any value of the thickness to width ratio definitely validates our bidimensional approach and the associate program. It is noteworthy to mention that this latter restitutes, in a single calculation, all the types of resonance modes: thickness, lateral, and bar modes.

B. Model exploitation

We propose here to illustrate the capabilities of our approach with regard to a 2 μm thick and 200 μm wide lossy resonator. The losses are incorporated through a complex normalized elastic stiffness as described previously thanks to the quality factor $Q_u = 1/\bar{\eta}_{33} = 1912.8$.

The Fig. 5 shows the calculated normalized admittances for two BAW resonators, laterally bounded and unbounded, respectively. The laterally bounded resonator exhibits parasitic lateral resonances. The computation time, for 1200 points and truncation orders $M=N=9$, is about 5 min for an ordinary laptop computer: CPU Intel Pentium IV and memory size 1 GB. This allows to consider, with our approach, rapid and precise optimization of resonators, whatever the thickness/width ratio value.

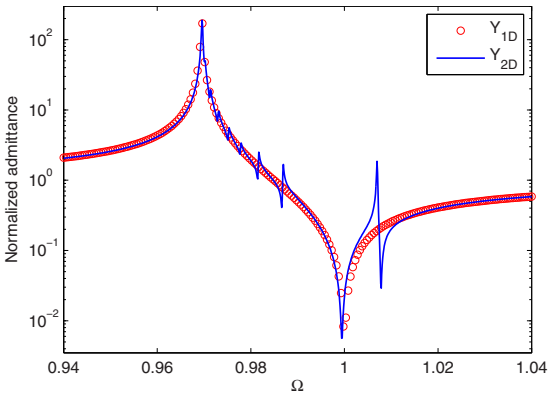

FIG. 5. (Color online) 1D and 2D normalized admittances of ZnO lossy resonators.

TABLE IX. Normalized resonance and antiresonance frequencies of ZnO resonator (L_1=200 μm and L_3=2 μm).

Modes	Resonance	Antiresonance
1	0.9696	0.9701
3	0.9730	0.9752
5	0.9770	0.9816
7	0.9867	0.9904
9	0.9995	1.0070

The Table IX shows the resonance and antiresonance frequencies of ZnO resonator with truncation orders $M=N=9$. Modal results are consistent with harmonic ones. The Fig. 6 shows the particle displacement profiles at the normalized resonance frequencies 0.9696 and 0.9730, respectively. The top figure displays the main thickness resonance, the bottom one displays the main thickness resonance along with a lateral spurious mode.

For a laterally bounded resonator, according to Rosenbaum,[13] the resonance frequencies are given by:

$$f_r^{m,n} \cong \frac{mV_L}{2L_3}\left[1+\left(\frac{nL_3}{mL_1}\right)^2\right]^{1/2}, \tag{17}$$

where V_L represents the velocity of the longitudinal mode. If $L_1 \gg L_3$, as in our previous illustration, the resonance frequency for the first mode ($m=1$) is given by:

$$f_r^{1,n} \cong \frac{mV_L}{2L_3}\left[1+\frac{n^2}{2}\left(\frac{L_3}{L_1}\right)^2\right], \quad n=1,3,\ldots. \tag{18}$$

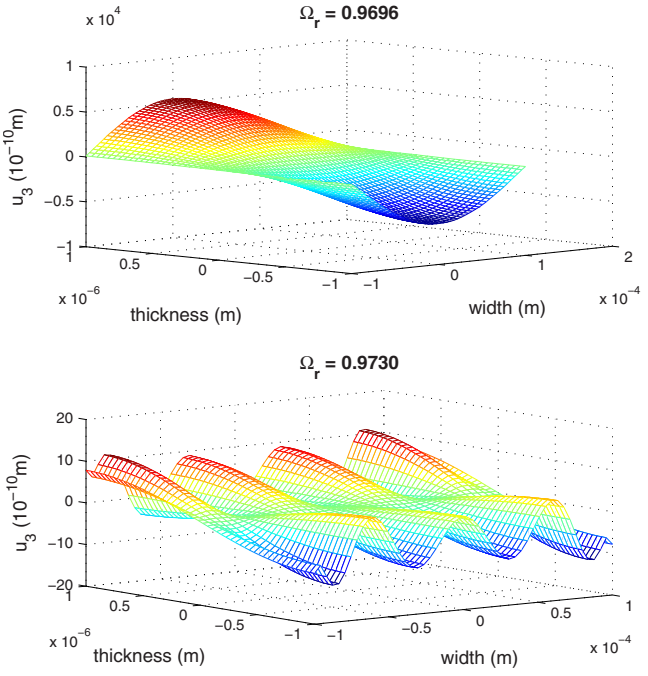

FIG. 6. (Color online) Particle displacement u_3 profiles into ZnO resonator for Ω_r=0.9696 and Ω_r=0.9730.

Our method and the associated program provide an optimization tool by which it is possible to choose the lateral dimensions to remove the spurs from the operating region of interest.

IV. SUMMARY

In this paper, we have extended the Legendre polynomial approach to study 2D structures with full metallization in order to take into account the lateral resonances. The description of the structure, the boundary conditions, and the electrical voltage source are directly incorporated into the propagation equations yielding a unique formalism allowing both harmonic and modal analyses. All the types of resonance, thickness modes, bar modes, anharmonic modes, whatever the thickness to width ratio value, are restituted through a single calculation. The approach was validated by comparing its predictions with results from literature or approached analytical models. The ZnO resonator was dealt with as an illustrative example in order to emphasize the capabilities of the method with regard to spurious modes in laterally bounded resonators. The method may be extended to partially metalized resonator. It is hoped to consider this problem in a subsequent paper.

APPENDIX: MATRICES OF THE INFINITE SYSTEM OF LINEAR EQUATIONS

$$AA^{11}_{jmkn} = \zeta^2 \bar{c}_{11} J5^0_{jm} J1^0_{kn} + \bar{c}_{55} J1^0_{jm} J5^0_{kn},$$

$$AA^{13}_{jmkn} = \zeta(\bar{c}_{13} J4^0_{jm} J2^0_{kn} + \bar{c}_{55} J2^0_{jm} J4^0_{kn}),$$

$$AA^{31}_{jmkn} = \zeta(\bar{c}_{13} J2^0_{jm} J4^0_{kn} + \bar{c}_{55} J4^0_{jm} J2^0_{kn}),$$

$$AA^{33}_{jmkn} = \zeta^2 \bar{c}_{55} J5^0_{jm} J1^0_{kn} + \bar{c}_{33} J1^0_{jm} J5^0_{kn},$$

$$BB^1_{jmkn} = \frac{\zeta}{r}[\bar{e}_{15} J2^0_{jm}(J4^2_{kn} - J4^0_{kn}) + \bar{e}_{31} J4^0_{jm}(J2^2_{kn} - J2^0_{kn})],$$

$$BB^3_{jmkn} = \frac{\zeta^2 \bar{e}_{15}}{r} J5^0_{jm}(J1^2_{kn} - J1^0_{kn}) + \frac{\bar{e}_{33}}{r} J1^0_{jm}(J5^2_{kn} - J5^0_{kn}),$$

$$CC^1_{jmkn} = r\zeta(\bar{e}_{15} J4^0_{jm} + \bar{e}_{31} J2^0_{jm}) J2^0_{kn},$$

$$CC^3_{jmkn} = r(\zeta^2 \bar{e}_{15} J5^0_{jm} J1^0_{kn} + \bar{e}_{31} J1^0_{jm} J3^0_{kn}),$$

$$DD_{jmkn} = \zeta^2[\bar{\varepsilon}_{11} J5^0_{jm}(J1^2_{kn} - J1^0_{kn}) + \bar{\varepsilon}_{33} J1^0_{jm}(J3^2_{kn} - J3^0_{kn})],$$

$$EE^1_{jk} = \frac{\zeta}{r} \bar{e}_{31} J4^0_{j0} J2^3_{k0}, \quad EE^3_{jk} = \frac{\bar{e}_{33}}{r} J1^0_{j0} J5^3_{k0},$$

$$FF_{jk} = J1^{-1,1,0}_{j0} J3^{-1,1,3}_{k0}; \quad MM_{jmkn} = \frac{\pi^2}{4} J1^{-1,1,0}_{jm} J1^{-1,1,0}_{kn},$$

$$NN^{11}_{jmkn} = \zeta^2 \bar{\eta}_{11} J5^0_{jm} J1^0_{kn} + \bar{\eta}_{55} J1^0_{jm} J5^0_{kn},$$

$$NN^{13}_{jmkn} = \zeta(\bar{\eta}_{13} J4^0_{jm} J2^0_{kn} + \bar{\eta}_{55} J2^0_{jm} J4^0_{kn}),$$

$$NN^{31}_{jmkn} = \zeta(\bar{\eta}_{13} J2^0_{jm} J4^0_{kn} + \bar{\eta}_{55} J4^0_{jm} J2^0_{kn}),$$

$$NN^{33}_{jmkn} = \zeta^2 \bar{\eta}_{55} J5^0_{jm} J1^0_{kn} + \bar{\eta}_{33} J1^0_{jm} J5^0_{kn},$$

$$GG^1_{mn} = \zeta e_{31} J2^{-1,1,0}_{0m} J1^{-1,1,0}_{0n}; \quad GG^2_{mn} = \bar{e}_{33} J1^{-1,1,0}_{0m} J2^{-1,1,0}_{0n}$$

$$J1^0_{jm} = \int_{-1}^{1} Q^*_j(q)\Pi(q)Q_m(q)dq = \frac{\sqrt{(2j+1)(2m+1)}}{2} \frac{(2j)!}{2^j(j!)^2} \frac{(2m)!}{2^m(m!)^2} \times \left[\frac{\chi_j \chi_m}{j+m+1} z^{j+m+1} + \frac{\chi_{j-2}\chi_m + \chi_j \chi_{m-2}}{j+m-1} z^{j+m-1} \right]_{-1}^{+1},$$

where

$$\chi_{j-n} = (-1)^{n/2} \frac{j(j-2)\ldots(j-n+1)}{2.4\ldots n\,.\,(2j-1)(2j-3)\ldots[2j-(n-1)]},$$

$$J1^{\gamma+1}_{jm} = \int_{-1}^{1} Q^*_j(q)\Pi(q)q^\gamma Q_m(q)dq = g(m+1)J1^\gamma_{jm+1} + g(m)J1^\gamma_{jm-1},$$

where

$$g(m) = \frac{m}{\sqrt{(2m-1)(2m+1)}},$$

$$J2^0_{jm} = \int_{-1}^{1} Q^*_j(q)\Pi(q)\frac{\partial Q_m}{\partial q}dq = \sqrt{2m+1}[\sqrt{2m-1}J1^0_{jm-1} + \sqrt{2m-5}J1^0_{jm-3} + \ldots],$$

$$J2^{\gamma+1}_{jm} = \int_{-1}^{1} Q^*_j(q)\Pi(q)\frac{\partial}{\partial q}[q^\gamma Q_m(q)]dq = g(m+1)J2^\gamma_{jm+1} + g(m)J2^\gamma_{jm-1},$$

$$J3^0_{jm} = \int_{-1}^{1} Q^*_j(q)\Pi(q)\frac{\partial^2 Q_m}{\partial q^2}dq = \sqrt{2m+1}[\sqrt{2m-1}J2^0_{jm-1} + \sqrt{2m-5}J2^0_{jm-3} + \ldots],$$

$$J3^{\gamma+1}_{jm} = \int_{-1}^{1} Q^*_j(q)\Pi(q)\frac{\partial^2}{\partial q^2}[q^\gamma Q_m(q)]dq = g(m+1)J3^\gamma_{jm+1} + g(m)J3^\gamma_{jm-1},$$

$$J4^0_{jm} = \int_{-1}^{1} Q^*_j(q)\frac{\partial}{\partial q}[\Pi(q)Q_m(q)]dq = Q^*_j(-1)Q_m(-1) - Q^*_j(1)Q_m(1) + J2^0_{jm},$$

$$J4^{\gamma+1}_{jm} = \int_{-1}^{1} Q^*_j(q)\frac{\partial}{\partial q}[\Pi(q)q^\gamma Q_m(q)]dq = g(m+1)J4^\gamma_{jm+1} + g(m)J4^\gamma_{jm-1},$$

$$J5^{0}_{jm} = \int_{-1}^{1} Q^{*}_{j}(q)\frac{\partial}{\partial q}\left[\Pi(q)\frac{\partial Q_m}{\partial q}\right]dq$$

$$= \sqrt{2m+1}\left[\sqrt{2m-1}J4^{0}_{jm-1} + \sqrt{2m-5}J4^{0}_{jm-3} + \ldots\right],$$

$$J5^{\gamma+1}_{jm} = \int_{-1}^{1} Q^{*}_{j}(q)\frac{\partial}{\partial q}\left\{\Pi(q)\frac{\partial}{\partial q}[q^{\gamma}Q_m(q)]\right\}dq$$

$$= g(m+1)J5^{\gamma}_{jm+1} + g(m)J5^{\gamma}_{jm-1},$$

[1] V. Plessky, Proc.-IEEE Ultrason. Symp. **1**, 195 (1993).
[2] S. Ballandras, M. Wilm, P.-F. Edoa, A. Soufrane, and V. Laude, J. Appl. Phys. **93**, 702 (2003).
[3] C. F. Campbell and R. J. Weber, Proc.-IEEE Ultrason. Symp. **1**, 477 (1992).
[4] R. Lerch, IEEE Trans. Ultrason. Ferroelectr. Freq. Control **37**, 233 (1990).
[5] A. Raherison, F. E. Ratolojanahary, J. E. Lefebvre, L. Elmaimouni, and T. Gryba, J. Appl. Phys. **104**, 014508 (2008).
[6] L. Elmaimouni, J. E. Lefebvre, A. Raherison, and F. E. Ratolojanahary, Ferroelectrics **372**, 115 (2008).
[7] T. Makkonen, A. Holappa, J. Ellä, and M. M. Salomaa, IEEE Trans. Ultrason. Ferroelectr. Freq. Control **48**(5), 1241 (2001).
[8] S. Datta and B. J. Hunsinger, J. Appl. Phys. **49**, 475 (1978).
[9] Y. Kim and W. D. Hunt, J. Appl. Phys. **68**, 4993 (1990).
[10] J. E. Lefebvre, V. Zhang, J. Gazalet, and T. Gryba, J. Appl. Phys. **85**, 3419 (1999).
[11] A. Raherison, Ph.D. thesis, Université de Valenciennes and Université de Fianarantsoa, 2009.
[12] R. L. Jungerman, P. Bennett, A. R. Selfridge, B. T. Khuri-Yakub, and G. S. Kino, J. Acoust. Soc. Am. **76**, 516 (1984).
[13] J. F. Rosenbaum, *Bulk Acoustic Wave Theory and Devices* (Artech, Boston, 1998).